Biogeosciences, 19, 3775–3789, 2022
https://doi.org/10.5194/bg-19-3775-2022

Biogeosciences
Open Access
EGU

Benthic alkalinity fluxes from coastal sediments of the Baltic and North seas: comparing approaches and identifying knowledge gaps

Bryce Van Dam[1], Nele Lehmann[1,4,7], Mary A. Zeller[3], Andreas Neumann[1], Daniel Pröfrock[2], Marko Lipka[3], Helmuth Thomas[1,5], and Michael Ernst Böttcher[3,6,7]

[1]Institute of Carbon Cycles, Helmholtz-Zentrum Hereon, Geesthacht, Germany
[2]Institute of Coastal Environmental Chemistry, Helmholtz-Zentrum Hereon, Geesthacht, Germany
[3]Geochemistry & Isotope Biogeochemistry, Leibniz Institute for Baltic Sea Research (IOW), Warnemünde, Germany
[4]Alfred Wegener Institute, Helmholtz Centre for Polar and Marine Research, Potsdam, Germany
[5]Institute for Chemistry and Biology of the Marine Environment (ICBM), University of Oldenburg, Oldenburg, Germany
[6]Marine Geochemistry, University of Greifswald, Greifswald, Germany
[7]Interdisciplinary Faculty, University of Rostock, Rostock, Germany

Correspondence: Bryce Van Dam (bryce.dam@hereon.de)

Received: 6 April 2022 – Discussion started: 7 April 2022
Revised: 27 June 2022 – Accepted: 2 July 2022 – Published: 19 August 2022

Abstract. Benthic alkalinity production is often suggested as a major driver of net carbon sequestration in continental shelf ecosystems. However, information on and direct measurements of benthic alkalinity fluxes are limited and are especially challenging when biological and dynamic physical forcing causes surficial sediments to be vigorously irrigated. To address this shortcoming, we quantified net sediment–water exchange of alkalinity using a suite of complementary methods, including (1) ^{224}Ra budgeting, (2) incubations with ^{224}Ra and Br^- as tracers, and (3) numerical modeling of porewater profiles. We choose a set of sites in the shallow southern North Sea and western Baltic Sea, allowing us to incorporate frequently occurring sediment classes ranging from coarse sands to muds and sediment–water interfaces ranging from biologically irrigated and advective to diffusive into the investigations. Sediment–water irrigation rates in the southern North Sea were approximately twice as high as previously estimated for the region, in part due to measured porewater ^{224}Ra activities higher than previously assumed. Net alkalinity fluxes in the Baltic Sea were relatively low, ranging from an uptake of −35 to a release of 53 µmol m^{-2} h^{-1}, and in the North Sea they were from 1 to 34 µmol m^{-2} h^{-1}. Lower-than-expected apparent nitrate consumption (potential denitrification), across all sites, is one explanation for our small net alkalinity fluxes measured. Carbonate mineral dissolution and potentially precipitation, as well as sulfide re-oxidation, also appear to play important roles in shaping net sediment–water fluxes at locations in the North Sea and Baltic Sea.

1 Introduction

Continental shelf systems are considered to act as sinks for atmospheric CO_2 (Borges et al., 2005; Laruelle et al., 2010, 2018; Rutherford et al., 2021), with an important but currently uncertain role in the global carbon budget (Lacroix et al., 2021). Current trends in shelf CO_2 uptake are highly variable (Laruelle et al., 2018), in response to a variety of factors, including regional trajectories in primary production, acid-base buffering (Thomas et al., 2007), the underlying geology, mixing with riverine and open-ocean waters, and wind patterns (Meyer et al., 2018). Where water depths are relatively shallow, there is increased potential for benthic–pelagic coupling to affect the net shelf CO_2 uptake. In regions like the shallow southern North Sea, persistent wind- and tidal-driven mixing strongly impacts both the benthic and the pelagic ecosystems. This mixing ventilates surface sediments, supplying oxidants for the respiration of organic matter and flushing out the reduced products, thereby affecting net sediment–water exchange of dissolved inorganic carbon (DIC) and total alkalinity (TA). Aerobic remineraliza-

tion is a key DIC source in physically or biologically ventilated surface sediments (Neumann et al., 2021; Rassmann et al., 2020), followed by microbial sulfate reduction (MSR; Al-Raei et al., 2009). These DIC sources may be further enhanced to varying extents by anaerobic processes like denitrification, as well as iron and manganese reduction, which, like MSR, also produce TA and DIC (e.g., Zeebe and Wolf-Galdrow, 2001). While intense biological reworking limits net organic carbon storage in North Sea sediments (Diesing et al., 2020; de Haas et al., 1997), net carbon uptake from the atmosphere may be possible through a combination of the shelf CO_2 pump (Thomas et al., 2004), as facilitated by large oceanic inflows (Lacroix et al., 2021), and a long-term increase in the DIC inventory driven by combined biological and anthropogenic CO_2 (Clargo et al., 2015).

Additionally, there is a suite of geochemical processes which may also affect net shelf CO_2 uptake. For example, the precipitation and dissolution of calcium carbonate ($CaCO_3$) and silicate minerals, pyrite formation and oxidation, dissolution and formation of silicate minerals, and reverse weathering may substantially affect net sediment–water fluxes of DIC and TA and, hence, the carbonate chemistry of the overlying water column (Berelson et al., 2019; Hagens et al., 2015; Pätsch et al., 2018; Rassmann et al., 2020; Thomas et al., 2009; Winde et al., 2017; Schwichtenberg et al., 2020). While these dissolution and precipitation processes are largely abiotic, their rates are shaped by the redox and acid-base setting, which itself is strongly biologically mediated (Morse and Mackenzie, 1990). Therefore, a strong interplay exists in shelf sediments between biogeochemical cycling of macro-nutrients and minor nutrients and benthic (bio)geochemical solid–solution interactions, all of which is further mediated by wind- and tidal-driven physical mixing.

Substantial prior work in the coastal North Sea shows that these sediment (bio)geochemical processes exert a strong cumulative effect on water-column carbonate chemistry (Brenner et al., 2016; Burt et al., 2014) and ultimate CO_2 exchange with the atmosphere (Thomas et al., 2009). Recent modeling and experimental efforts point to benthic denitrification of riverine nitrate as a dominant TA source to the southern North Sea but also imply a substantial role of benthic carbonate mineral dissolution (Winde et al., 2014a; Pätsch et al., 2018; Burt et al., 2016; Schwichtenberg et al., 2020). In addition to these processes, metal (Fe and Mn) reduction can also be an important TA source, especially in depositional centers with finer-grained sediment and greater organic carbon loads (Lenstra et al., 2019; Reithmaier et al., 2021). However, rapid sediment accumulation may decouple net Fe reduction from sediment–water TA fluxes (Rassmann et al., 2020), and reaction kinetics of carbonates under the impact of dissolved Fe and Mn may be slowed down substantially (Dromgoole and Walter, 1990; Böttcher and Dietzel, 2010). Hence, more investigations of the benthic (bio)geochemical processes in relation to benthic DIC/TA fluxes is clearly warranted.

The Baltic and North seas form a continuum of water and material transport (Gustafsson, 1997; Kuliński et al., 2022; Maar et al., 2011), deeply linking the carbon cycles of these two ocean basins. While the nearshore regions of the southern North and western Baltic seas are located at a similar latitude, have a similar water depth, and contain similar sediment types, they experience very different physical forcing. While tidal forcing dominates in the southern North Sea, the western Baltic is instead characterized by negligible tidal forcing, estuarine mixing, and associated salinity variability. For example, large tidal forcing combined with coarse-grained sediments in the southern North Sea could promote advective over diffusive fluxes and increase the oxygen penetration depth (Billerbeck et al., 2006; Al-Raei et al., 2009). Bioturbation and bioirrigation are also especially important in the coastal North Sea and can explain how sediment–water fluxes of oxygen and other elements vary across season and sediment type (Lipka et al., 2018; Gogina et al., 2018; Neumann et al., 2021; Bratek et al., 2020). In contrast, limited tidal forcing combined with finer-grained sediments in the western Baltic Sea could promote stronger biogeochemical zonation and a greater importance of anaerobic over aerobic processes (Böttcher et al., 2000). While we know that these factors shape benthic biogeochemical processing, sediment–water fluxes in these shallow coastal environments are still poorly constrained, limiting our understanding of their role in the regional carbon cycle (Kuliński et al., 2022).

In this study, we present new results quantifying sediment–water DIC and TA fluxes in the southern North Sea, considering a variety of methods, including Ra budgets and core incubations. This dataset is augmented by archived porewater data from the Baltic Sea and some additional sites in the North Sea in order to further understand the differential impacts of physical and biogeochemical forcing in these two neighbouring basins. Benthic TA, DIC, and element fluxes were modeled from these porewater profiles, aimed at predicting net sediment–water fluxes of DIC and TA across a broad range in sediment types. The relationships of especially SO_4^{2-}, DIC, TA, Fe, and PO_4^{3-} were utilized as a first approach to the potential role of secondary (bio)geochemical processes described above, which have so far only been poorly represented in regional carbon budgets (Pätsch et al., 2018; Schwichtenberg et al., 2020), in the context of the coupled physical and biological drivers of net benthic–pelagic coupling. Each applied method has its own advantages and disadvantages to emphasize advection, diffusion, or bioirrigation to varying degrees. The differences between the approaches are partially related to methodological limits but may also indicate real differences between the consequences of physical and biological drivers for biogeochemical processes such as net CO_2 uptake and, therefore, require further investigations.

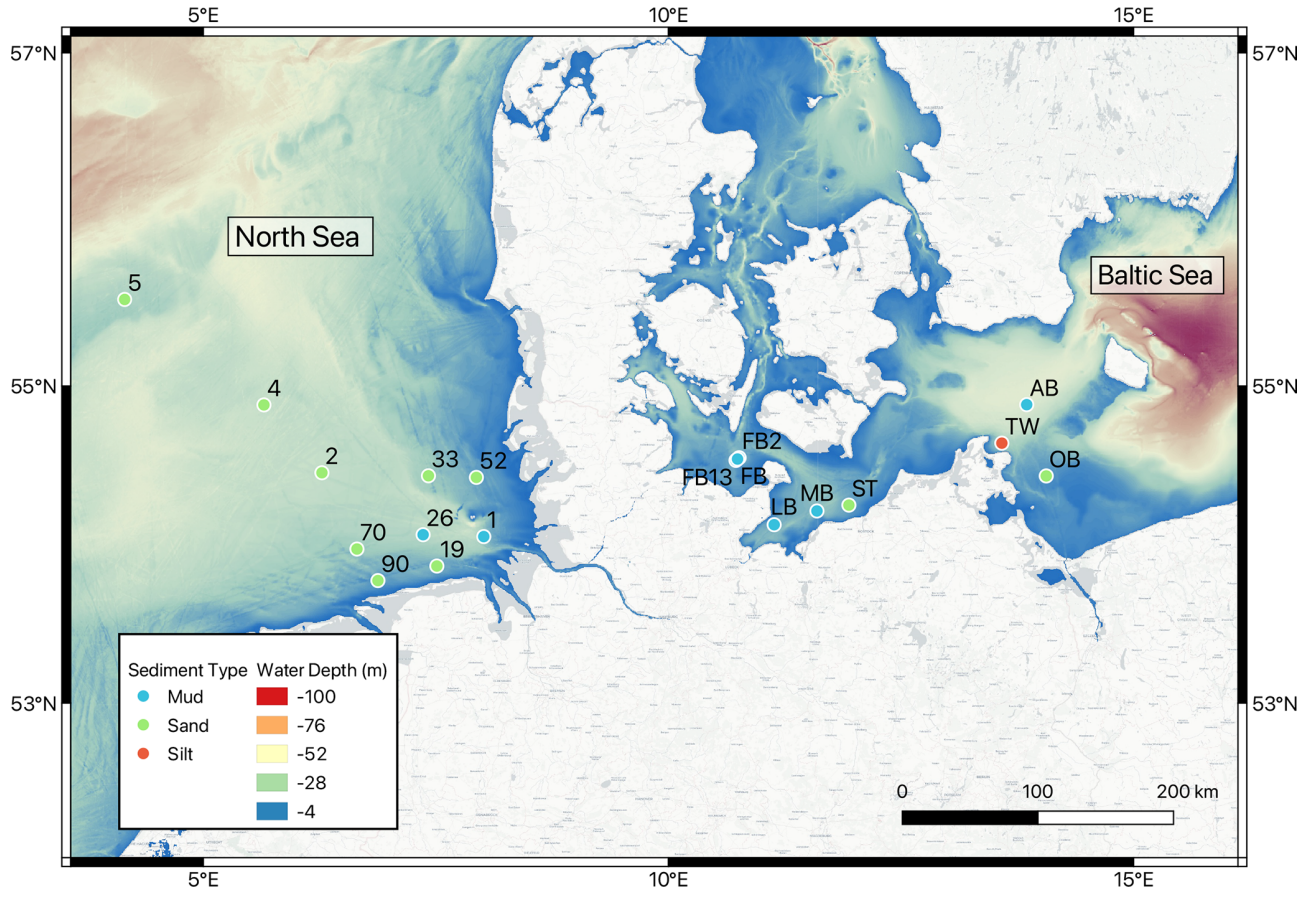

Figure 1. Map of sampled stations, with points colored by sediment type.

2 Methods

2.1 Dataset description

Samples collected for this study come from a set of 19 stations in the southern North Sea (10 sites) and the western Baltic Sea (9 sites) that were visited during cruises between 2015 and 2020 (Fig. 1). Here we present results from four cruises where sampling and experimental approaches are comparable; these were HE541 (September 2019) and MSM50a (January 2016) in the North Sea and EMB111 (August–September 2015) and EMB238 (May 2020) in the Baltic Sea. Parts of the experimental results from MSM50a and EMB111 have previously been published by Lipka et al. (2018) and Gogina et al. (2018), and these sites were chosen to be complementary in terms of water depth, distance from shore, and sediment type. Only results from HE541 in the southern North Sea are used for the Ra budget and core incubations, while porewater profile modeling and constituent ratio analyses are given for all sites. The water depth at these sites is shallow at 23.6 ± 8.5 m (mean $\pm$ SD), with a maximum of 46.0 m (Site AB) and minimum of 11.2 m (Site 52). Of the 19 stations considered here, 10 are classified as sandy sediments, 8 as muds, and 1 as silt sediment (Lipka, 2017; Lipka et al., 2018).

At each site, a multicoring device was used to collect 10 cm diameter cores which contained approximately 20 cm of sediment. Sediment porewaters were extracted within 6 h of core collection using Rhizons (nominal pore size of 0.15 µm) at 1–2 cm intervals for the first 10 cm and with a typical interval of 5 cm below that. Table S1 in the Supplement lists the preservation techniques and measurement methods for each analyzed parameter.

2.2 Laboratory analyses

The samples taken during the HE541 cruise were analyzed according to the following protocols: TA was determined at the Leibniz Institute for Baltic Sea Research (IOW) via small-volume (400–800 µL), two-point potentiometric titration according to van den Berg and Rogers (1987). The sample was transferred into a vial with a pre-set volume of HCl on board, assuming that all weak acids in solution would be protonated (pH < 3). The sample was cooled at 4 °C until further analysis. Back in the lab, the sample was allowed to equilibrate to room temperature and the first potentiometric point was measured using a pH meter (SevenMulti, Met-

tler Toledo, Giessen, Germany). After the addition of HCl (75 µL, 0.1 M), the second point was recorded (pH ≈ 2). Taking these two points, the slope of the electrode response was determined (van den Berg and Rogers, 1987). The measurements were calibrated against certified reference materials (CRMs), from batch 142 provided by Andrew Dickson (Scripps Institution of Oceanography, San Diego, California, USA).

DIC and δ^{13}C-DIC were also analyzed at IOW with continuous-flow isotope-ratio-monitoring mass spectrometry (CF-irmMS) using a gas mass spectrometer (Finnigan MAT 253, Thermo Fisher Scientific, Waltham, Massachusetts, USA) coupled to a gas bench (GasBench II, Thermo Fisher Scientific, Waltham, Massachusetts, USA) via a continuous-flow interface (ConFlo IV, Thermo Fisher Scientific, Waltham, Massachusetts, USA) (Winde et al., 2014a). A calibration of the instrument was performed against CRMs provided by Andrew Dickson (Scripps Institution of Oceanography, San Diego, USA). Sulfide concentrations were measured at IOW using the methylene blue technique (Cline, 1969) on a Specord 40 spectrophotometer (Analytik Jena, Germany).

Determination of elemental concentrations (Ca, Fe, Mn, P, S) was performed at Hereon using an ICP-MS/MS (Agilent 8800, Agilent Technologies, Tokyo, Japan) coupled to an ESI SC-4 DX FAST autosampler (Elemental Scientific, Omaha, Nebraska, USA) equipped with a discrete sampling system with a loop volume of 1.5 mL (Zimmermann et al., 2020). Measurements were validated with a seawater standard ($S = 35$, IAPSO Standard Seawater, Ocean Scientific International Ltd, Hampshire, United Kingdom) with the addition of Fe and Mn ($c = 1\,\mathrm{mg\,L^{-1}}$). Calibrations were prepared from either single- or multi-element solutions traceable to NIST CRMs. Nutrient concentrations were determined using an automated continuous-flow system (AA3, Seal Analytical, Norderstedt, Germany) and standard colorimetric techniques (Graßhoff and Almgren, 1983). Dissolved-metal, S, P, and Si results from the Baltic Sea samples were measured at IOW via inductively coupled plasma optical emission spectrometry (ICP-OES) as described by Winde et al. (2014a) and Lipka et al. (2018).

2.3 Sediment–water flux determinations

In this study, we applied three independent methods to estimate sediment–water fluxes of major, minor, and trace elements. This is a conservative approach because each individual method emphasizes advective or diffusive processes to a different degree, ensuring that our calculated sediment–water fluxes span a complete range in possible rates.

First, a water-column ^{224}Ra decay balance is used to derive porewater irrigation rates, which are in turn used to parameterize bulk sediment–water fluxes based on measured concentrations in the upper porewaters. The second approach is similar to the first but with irrigation rates derived from shipboard core incubation experiments, with both bromide and ^{224}Ra employed as tracers. We also used PROFILE models to assess sediment–water fluxes for all sites, which use the shape of porewater profiles to balance internal production and consumption with vertical diffusive transport (Berg et al., 1998).

2.3.1 ^{224}Ra decay balance

Samples for ^{224}Ra were collected exclusively during the HE541 cruise in the southern North Sea, following the methods of Moore et al. (2011) and Burt et al. (2016) (^{224}Ra determinations were not made during the other cruises). Briefly, approximately 100 L of water from the ship's seawater line was passed through a cascade of 10 and 1 µm filters and then pumped slowly ($1\,\mathrm{L\,min^{-1}}$) through a cartridge containing manganese-oxide-coated fibers which quantitatively adsorb Ra (confirmed with efficiency samples). After rinsing and drying, samples were counted first within 24 h of collection on board the ship with a radium delayed coincidence counting (RaDeCC) system (Moore and Arnold, 1996). A second count was executed after 7–14 d, allowing us to apply the error propagation technique of Burt et al. (2016) to derive uncertainty statistics for the final ^{224}Ra activities given in Sect. 3.1. In addition to the bulk seawater samples, porewaters were also collected from all sites during the HE541 cruise using Rhizons, with water from all core depths combined into a single sample (∼ 100–200 mL) that was treated and counted on a RaDeCC as described above.

Because ^{224}Ra is not a gas and has a relatively short half-life (3.7 d), its activity in surface waters is a relatively simple balance between advective–diffusive inputs from the sediments (where it decays from its longer-lived parent isotope ^{228}Th), lateral exchange in surface waters, and radioactive decay (Garcia-Orellana et al., 2021). We assume that lateral exchange is a small term in this budget, allowing us to calculate the benthic advective–diffusive input term (net irrigation) as the balance between radioactive decay and the measured surface water activity. These irrigation rates derived from the ^{224}Ra decay balance ($\mathrm{mean} = 81\,\mathrm{L\,m^{-2}\,d^{-1}}$) were then used to calculate net sediment–water fluxes by multiplying by the average concentration difference between the porewater and the overlying water concentration. For "sandy" sites, we applied the average porewater concentration of each parameter from the upper 5 cm in each core, while a single concentration from the top sediment layer of each core was used for the "muddy" and "silty" sites. The sign convention is that positive fluxes indicate a flux out of the sediment and vice versa.

2.3.2 Shipboard incubations

Benthic fluxes were measured on intact sediment cores from a multicorer by means of whole-core batch incubations. Typically, three to four intact sediment cores in transparent plastic

Table 1. Parameterization of the PROFILE model.

		Sand	Silt	Mud
Max deviation when accepting value (%)			0.001	
Level of significance for F statistic			0.2	
Biodiffusivity ($cm^2\,h^{-1}$)	< 5 cm	0.36	0.18	0.18
	5–10 cm	0.18	0	0
	> 10 cm	0	0	0
Irrigation coefficient (h^{-1})	< 5 cm	0.11	0.0011	0.0011
	5–10 cm	0.011	0	0
	> 10 cm	0	0	0
Porosity (φ)		0.4	0.6	0.8
Coefficient of molecular diffusivity ($cm^2\,h^{-1}$)		Calculated in R: "marelac" as f(Sal, Temp, Pres)		
Sediment diffusivity ($cm^2\,h^{-1}$)		$D_s = D/(1+3[1-\varphi])$		
Boundary conditions		Concentration and diffusive flux at the bottom		

liners (PMMA, 10 cm inner diameter, 60 cm length) per station were selected, which had no visible perturbations such as cracks, voids, or injured animals. The sediment cores were typically 15–30 cm in length. The incubation was enclosed with a gastight lid that was adjusted to a resulting supernatant height of 15 cm (approximately 1 L volume). The water column was constantly stirred by horizontal propellers. The stirring intensity was adjusted to the highest intensity that did not result in sediment resuspension to ensure vigorous mixing of the supernatant and prevent suspended particles from settling. Incubations were executed aboard the research vessel in a temperature-controlled lab set to in situ temperature. Primary production was excluded by wrapping the cores in aluminum foil. At the beginning of each incubation, a NaBr solution was injected into the supernatant, which resulted in a final Br^- concentration of 1.6 mmol L^{-1}. During incubation, oxygen was monitored continuously to assess the progress, and the incubation was terminated when the oxygen saturation dropped below approximately 80 % (typically after 12 to 24 h). Water samples for nutrient and Br^- analyses were drawn from the core supernatant in 3–6 h intervals (typically 10 time steps) by means of syringes connected to PVC tubing. Water samples were then filtered through 0.45 µm syringe filters and stored frozen until analysis in the land-based laboratory. After incubations, additional samples from the supernatant were immediately taken for measurements of radium and DIC. The incubation method is described in detail in Neumann et al. (2021).

2.3.3 PROFILE modeling

We first employed the one-dimensional numerical model tool PROFILE to derive sediment–water fluxes and internal rates of production and consumption for most measured constituents (Berg et al., 1998). PROFILE builds a best-fit model from measured porewater profiles, assuming they are representative of steady-state conditions. This model is then split into several equidistant zones (typically 5 to 10 discrete intervals), each of which is fit with a specific net production rate. We then set a first boundary condition as the calculated diffusive flux out the bottom of the model domain, using the concentration gradient in the two deepest porewater samples, as well as the sediment porosity, and calculated the molecular diffusion coefficient (Table 1). The final sediment–water flux is then determined through conservation of mass between net internal production and the bottom diffusive flux. Further parameters needed to inform PROFILE include sediment porosity (φ), biodiffusivity, irrigation, diffusivity, statistical terms, and others given in Table 1. Biodiffusivity and irrigation coefficients were chosen through an iterative process, changing one variable at a time and comparing model performance for each sediment class.

3 Results and discussion

3.1 North Sea irrigation rates (decay balance and incubation)

Surface water ^{224}Ra activities were consistent throughout the southern North Sea, ranging from 262 ± 12.4 (Site 33) to 389 ± 22.1 dpm m^{-3} (Site 70). This is approximately twice as high as found in previous studies in the region (Burt et al., 2014, 2016) but similar to activities for the Wadden Sea (Moore et al., 2011). Our observation of high surface water ^{224}Ra is consistent with early-fall wind-driven vertical mixing causing an enhanced exchange between porewater high in ^{224}Ra and the surface water. The wind-driven water-column mixing also had the effect of breaking down any vertical stratification that may have developed during the summer (not shown). Our porewater ^{224}Ra activities (8.4 ± 0.85 to 44 ± 2.9 dpm L^{-1}, average of 19.9 dpm L^{-1} (or 19 946 dpm m^{-3})) were also approximately double compared to previous measurements in the German Bight (Burt

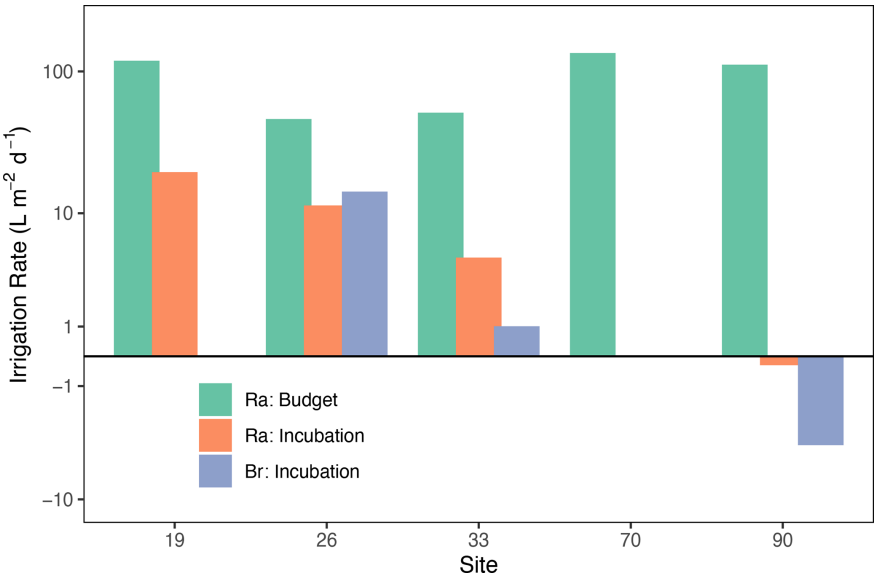

Figure 2. Porewater irrigation rates (L m^{-2} d^{-1}) for the North Sea only, derived from Ra budget (green) and incubations with Ra (orange) or bromide (blue) as tracers.

et al., 2014), and the Wadden Sea (Moore et al., 2011). These high ^{224}Ra activities yield calculated irrigation rates (mean = 92.5 L m^{-2} d^{-1}; green bars in Fig. 2) that were about twice the levels found by Burt et al. (2014). Solute fluxes for these sites are derived using PROFILE modeling, as discussed later. The high variability in porewater ^{224}Ra activity (8.4 to 44 dpm L^{-1}) also shows that care should be taken when deciding on endmember activities for ^{224}Ra-based budgets aimed at assessing porewater irrigation rates (Cook et al., 2018; Garcia-Orellana et al., 2021).

Irrigation rates derived from Br^- and ^{224}Ra measurements during the shipboard incubation experiments (mean = 8.9 L m^{-2} d^{-1}; blue bars) were a factor of 10 lower than rates derived from the ^{224}Ra decay balance. This is consistent with prior studies in the southern North Sea, where incubation-based fluxes were 2–3 times lower than decay-balance estimates (Burt et al., 2014). This difference is likely due to the fact that the decay balance implicitly represents the combined diffusive, advective, and bioirrigative processes that exist in the environment, which are incompletely captured in whole-core incubations. We must stress here that the Ra decay balance does not necessarily represent a better estimate of the real irrigation rate as many issues also exist with this method especially related to porewater endmember determination and the assumption of a steady state (Cook et al., 2018; Garcia-Orellana et al., 2021). Rather, these irrigation rates and solute fluxes, presented below, simply represent a most likely range in "real-world" values. The difference among approaches can also illustrate the varying importance of physical and bio-mediated forcing of net sediment–water exchange.

3.2 Net TA fluxes

3.2.1 North Sea TA fluxes from irrigation, incubation, and PROFILE modeling

Using the range in irrigation rates shown above, we calculated net sediment–water fluxes for a variety of solutes using the measured surface–porewater concentration difference (by convention, positive is out of the sediment). Average TA fluxes are tabulated in Table 2. At only two sites in the North Sea was porewater TA enriched enough to reliably calculate net fluxes using the incubation or budget approaches, given the relatively low precision of the small-volume TA titration method applied here. However, at these two sites (19 and 26), our TA fluxes (Fig. 3) were 1–2 orders of magnitude lower than previous estimates for this region (Brenner et al., 2016; Burt et al., 2014; Voynova et al., 2019). Excluding the PROFILE-modeled TA fluxes for the North Sea (which had very low R^2), net TA fluxes in the North Sea were relatively low, ranging from 1.1 to 6.7 µmol m^{-2} h^{-1} across all sites and sediment types (Table 2).

Burt et al. (2014) applied a similar Ra-based approach to estimate benthic fluxes but used a porewater–surface water TA difference of 0.7 mM, far greater than what we observed. For example, our porewater TA measurements at sites 19 and 26 were on average 2.23 and 2.26 mM, only 2–4 µM (0.002–0.004 mM) greater than bottom water TA, an insignificant difference considering the relatively low analytical precision of these small-volume TA titrations. As a result, the inferred sediment–water TA fluxes in Burt et al. (2014) were substantially larger than ours, at 196–921 µmol m^{-2} h^{-1}. Likewise, Voynova et al. (2019) estimated sediment–water TA fluxes in

Table 2. Comparison of average TA fluxes ($\mu mol\,m^{-2}\,h^{-1}$) between methods in the North and Baltic seas, separated by sediment type.

Basin	Method	Mud	Sand	Silt
Baltic Sea	PROFILE	53 ± 95.3 ($n = 6$)	-4.3 ± 43.5 ($n = 2$)	-35 ($n = 1$)
North Sea	PROFILE	1 ± 2.1 ($n = 3$)	33.6 ± 42.3 ($n = 5$)	–
North Sea	Ra incubation	1.5 ± 3.5 ($n = 2$)	1.1 ± 1.6 ($n = 2$)	–
North Sea	Ra budget	5.9 ± 14.2 ($n = 2$)	6.7 ± 9.4 ($n = 2$)	–
North Sea	Br incubation	1.8 ± 4.4 ($n = 2$)	–	–

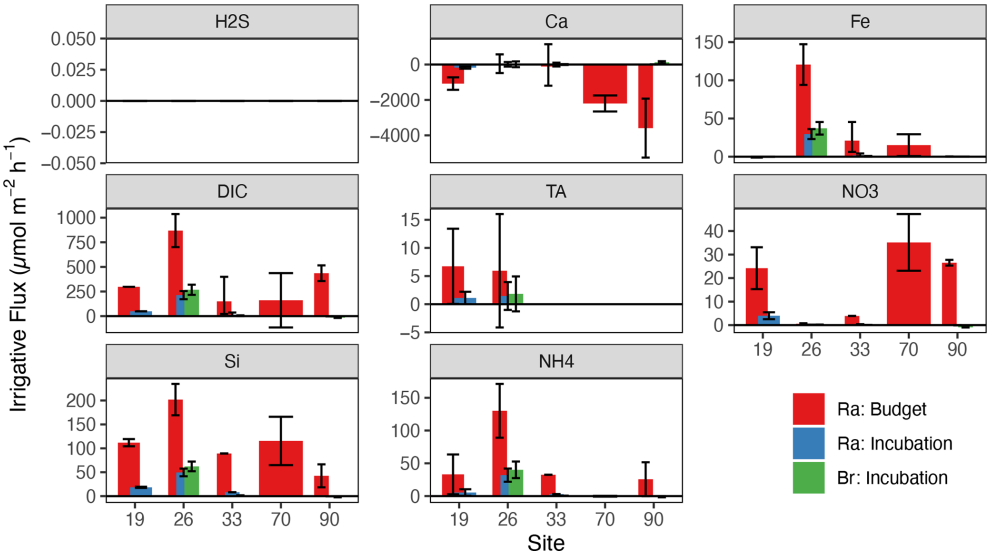

Figure 3. Average sediment–water fluxes ($\mu mol\,m^{-2}\,h^{-1}$) derived from Ra or Br^- incubation or Ra decay from the North Sea sites only. In this figure, the error bars represent minimum and maximum fluxes calculated from replicate porewater cores taken at each site.

the southern North Sea (based on observed seasonal variations in TA) to be more than 2 orders of magnitude higher, at 488–1117 $\mu mol\,m^{-2}\,h^{-1}$ (Table 1 in Voynova et al., 2019). Two recent modeling and empirical studies placed mean TA fluxes for this region at 83 (Pätsch et al., 2018) and 238–275 $\mu mol\,m^{-2}\,h^{-1}$ (Brenner et al., 2016), respectively, closer to but still greater than our results.

3.2.2 Baltic Sea TA fluxes from PROFILE modeling

In the Baltic Sea muddy sites AB and LB, TA concentration in surface sediments (0–10 cm depth) exceeded surface water TA by 1–10 mM, a significant excess considering the analytical precision of small-volume TA titrations. This excess TA caused PROFILE-modeled sediment–water TA fluxes in the Baltic Sea muddy sites AB and LB as high as 159 $\mu mol\,m^{-2}\,h^{-1}$ (Site LB, Fig. 4), while a smaller negative flux was observed at Site MB. Down-core trends in TA at these sites are well within measurement precision, allowing us to discuss potential sources of this TA and implications in Sect. 3.5. In contrast with the relatively large excess TA in surface sediments at the Baltic Sea muddy sites, TA was very close to the overlying water concentration in Baltic sandy and silty sites, where increases in porewater TA were not observed until depths of 10–15 cm. Resulting modeled TA flux was small and negative at the Baltic sandy and silty sites, at -4.3 and -35 $\mu mol\,m^{-2}\,h^{-1}$, respectively (Table 2 and Fig. 4). In contrast, PROFILE-modeled TA fluxes averaged across all Baltic Sea muddy sites for which fluxes could be calculated (AB, LB, MB) were 53 ± 95.3 $\mu mol\,m^{-2}\,h^{-1}$ (Table 2). This is approximately 50 % of the non-resolved "non-riverine" TA source from Gustafsson et al. (2014), which was implied to be driven largely by denitrification, sulfur metabolism, and silicate weathering. The minor down-core differences in TA in the Baltic Sea sandy sites are due to enhanced mixing in sediments with relatively low microbial activity. An analysis (Sect. 3.4–3.6) supports the following factors as key in sustaining low or negative net TA fluxes in sandy Baltic Sea sites: (1) low net denitrification and (2) complete re-oxidation of sulfide and Fe(II) in surface sediments.

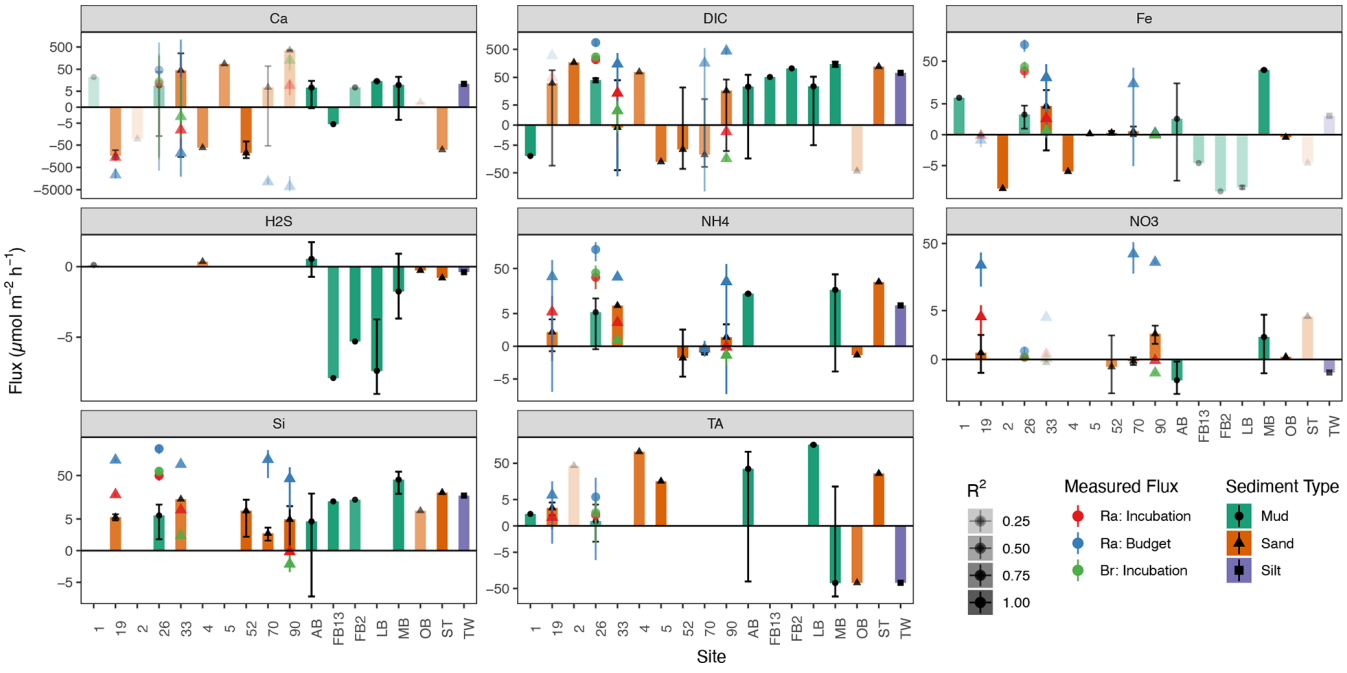

Figure 4. Sediment–water fluxes ($\mu mol\,m^{-2}\,h^{-1}$) for all sites in the Baltic (sites AB–TW) and North seas (sites 1–90), derived from PROFILE modeling (colored bars), with incubation and decay rates for comparison from the North Sea only (colored points). Bars with greater transparency indicate PROFILE flux results of lower confidence (R^2). The error bars in this figure represent the standard deviation of fluxes modeled from replicate cores at each site.

3.3 Sediment–water fluxes of other constituents (Baltic and North seas)

Net sediment–water fluxes are shown together in Fig. 4, with the bars representing average PROFILE-modeled fluxes, while the fluxes derived from incubation experiments and ^{224}Ra decay balances are depicted as the colored points. Typically, PROFILE-modeled fluxes were at least 10× smaller than fluxes derived from the ^{224}Ra decay balance. This is consistent with enhanced advective forcing that is captured by the decay-balance approach but missed by the incubation experiment and PROFILE model, which are in closer agreement. In addition to the sediment–water fluxes described above, the PROFILE model also generates estimates of net internal production/consumption, representing a superimposition of combined biological and abiotic sources/sinks in each model zone of the sediment (Fig. S2 in the Supplement).

Some solute fluxes exhibited similar trends across all sites in the North and Baltic seas. For example, Si fluxes were consistently positive (out of sediments) for all sites, across all methods (Fig. 4). In agreement with prior work in the region (Lipka et al., 2018; Gogina et al., 2018), ammonium (NH_4^+) release was also common and positive across all locations, except for three sandy sites in the North Sea (52, 70, 90). Net H_2S fluxes were not significantly different from zero in any North Sea sites, while PROFILE-modeled H_2S fluxes for three Baltic sites (FB2, FB13, and LB) were negative (into the sediment). We believe that these few large negative H_2S fluxes were created artificially by our use of a boundary condition (flux out of the bottom) that intersects with the zone of peak H_2S accumulation. In contrast, other modeled solute fluxes varied more between basins (North vs. Baltic) than across sites within basins. For example, TA fluxes in the North Sea sites were close to zero (albeit with low R^2), while PROFILE-modeled fluxes in the Baltic were larger in magnitude and more variable (Fig. 4). Baltic sites were also more often sources of Ca^{2+} to the water (except AB and FB13), while Ca^{2+} fluxes in the North Sea were more variable and statistically less robust.

PROFILE-modeled NO_3^- fluxes are variable and close to zero across all sites, in contrast to prior studies in the region suggesting net NO_3^- uptake by denitrification (Brenner et al., 2016). In fact, net NO_3^- fluxes derived from the incubation and Ra budget were positive (out of the sediment). This is in line with porewater NO_3^- trends, which generally show no net depletion in porewaters relative to surface water. While canonical denitrification is likely playing some role, the small NO_3^- fluxes in combination with larger NH_4^+ fluxes suggest the presence of dissimilatory nitrate reduction to ammonium (DNRA) as a secondary sink for NO_3^-, with denitrification fed by internally produced NO_3^- rather than allochthonous NO_3^-. Low net denitrification is consistent with slurry and flow-through core incubations in the German Bight showing denitrification largely supplied internally by nitrification (Marchant et al., 2016). In contrast, net

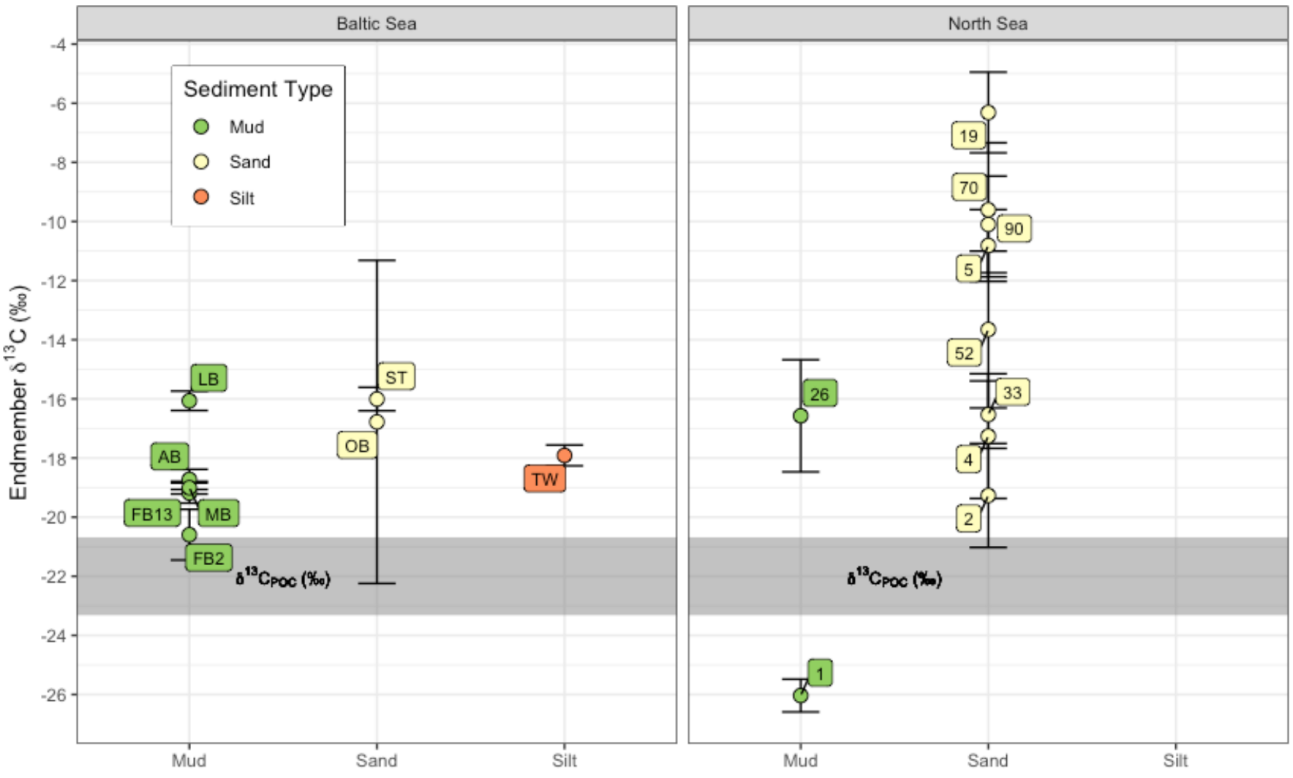

Figure 5. Potential endmember isotopic values for porewater DIC, derived from Miller–Tans plots of DIC $\times$ δ^{13}C-DIC vs. DIC (shown in Fig. S1 in the Supplement). The grey area represents a range in expected δ^{13}C-POC values for the North and Baltic seas combined, and the error bars represent the standard error of the Miller–Tans slope.

denitrification can be quite high at estuarine sites receiving "new" NO_3^- from the Elbe River, especially during the winter when river discharge is elevated (Neumann et al., 2017). Nevertheless, DNRA is a relatively minor process in the German Bight, limited mostly to intermediate (Marchant et al., 2016) and fine-grained sediment (Bratek et al., 2020). As such, it could also be that these NH_4^+ fluxes are a simple result of aerobic degradation of organic matter. Therefore, in contrast with prior studies in the region (Burt et al., 2014; Brenner et al., 2016; Voyanova et al., 2019), we suggest relatively low net denitrification rates, with limited potential for TA production. This is in line with De Borger et al. (2021) and Pätsch et al. (2018), who together indicate relatively low denitrification rates roughly balanced with nitrification, a feature that is supported by our low or negative modeled net TA fluxes (Fig. S2).

DIC flux was variable across sites but most often positive. Fluxes parameterized by Ra budgets and incubations agreed well with previously modeled diffusive fluxes for the region (Lipka, 2017, their Fig. 70), but our PROFILE model generated relatively low DIC fluxes. Sites with greater DIC release were also generally larger sources of Si, NH_4^+, and P, in line with the breakdown of algal detritus as a source for both.

3.4 Biogeochemical sources and sinks

3.4.1 δ^{13}C-DIC sources: Miller–Tans plots

The stable isotope composition of DIC reflects the diagenetic impact from the remineralization of particulate organic carbon (POC) and dissolved organic matter (DOM) as well as methane oxidation and interactions with carbonates (e.g., Ku et al., 1999; Meister et al., 2019; Wu et al., 2018). Using measured δ^{13}C-DIC data, we conducted a Miller–Tans plot analysis aimed at identifying isotopic endmembers as possible DIC sources (Fig. 5). In this graphical approach, the isotopic composition of DIC multiplied by its concentration is plotted against the concentration, with the slope indicative of the δ^{13}C-DIC source value, or endmember. If the remineralization of POC is the only source of DIC to porewaters, the slope of the Miller–Tans plot should be the same as the isotopic signature of δ^{13}C-POC, which in these sites ranges from -20 ‰ to -25 ‰ throughout the southern North Sea (Böttcher et al., 1998, 2000; Pollmann et al., 2021; Serna et al., 2014) and from -21 ‰ to -24 ‰ in the southwestern Baltic Sea (Böttcher et al., unpublished data; Voß and Struck, 1997). Any deviation in the y intercept from typical δ^{13}C-POC values may result from calcium carbonate dissolution

as an important modulator of DIC and TA fluxes (Winde, 2017).

Muddy or silty sites (1, 26, AB, FB13, FB2, LB, MB, TW) tend to have a larger range in DIC and so allow for a more robust graphical analysis. Calculated δ^{13}C-DIC endmembers for these sites were generally much higher (heavier) in comparison with the δ^{13}C-POC references listed above, ranging from −16 ‰ to −21 ‰ (Baltic Sea) and −17 ‰ to −26 ‰ (North Sea). That the δ^{13}C-DIC endmember at Site 1 in the North Sea (−26 ‰) is well below the δ^{13}C-POC source indicates a potential DIC input from methane oxidation. Elevated surface water methane concentrations have been previously observed near Site 1 in the region around Helgoland (Bussmann et al., 2021). Due to lower microbial activity (Al Raei et al., 2009) and enhanced porewater exchange (de Beer et al., 2005), the sandy sites have a smaller total range in DIC concentrations and isotope compositions, decreasing the confidence in a Miller–Tans plot approach. Some of the sandy sites (2, 33, 4, OB, and ST), however, yield a similar δ^{13}C-DIC endmember value when compared to the muddy sites with values ranging between −16 ‰ and −19 ‰. Other sandy sites (19, 5, 52, 70, 90) have much heavier endmembers, ranging from −6 ‰ to −12 ‰. This could suggest carbonate dissolution is contributing to heavier DIC values (Ku et al., 1999; Winde et al., 2014a, b; Wu et al., 2018). Carbonate weathering in porewaters has previously been suggested to be an important DIC and TA source (Winde et al., 2014a, b; Winde, 2017; Pätsch et al., 2018; Brenner et al., 2016). However, evidence for this is weak in our sandy North Sea sites, where porewater Ca^{2+} concentrations were low relative to overlying surface water, as seen in the generally negative Ca^{2+} fluxes (Figs. 3 and 4), indicating no significant net carbonate dissolution. Instead, these heavier δ^{13}C-DIC endmembers are likely reflective of $CaCO_3$ mineral dissolution and re-precipitation cycling (Walter et al., 2007).

3.4.2 DIC sources and sinks: process correlations

While the δ^{13}C-DIC source indicated by the Miller–Tans plot approach above may help to identify possible electron donors, it cannot provide information as to the terminal electron acceptors that were used to respire the organic carbon substrate. Microbial sulfate reduction (MSR) is an important mineralization process in marine sediments of this region (Jörgensen, 1989; Al-Raei et al., 2009) and leads to the production of DIC and TA (Zeebe and Wolf-Gladrow, 2001). Down-core correlations between DIC and SO_4^{2-} may indicate the relative extent by which MSR is associated with DIC (and TA) production. We calculated excess DIC and sulfate either (1) as the difference between porewater and bottom water measurements, when porewater salinity, as inferred by porewater K concentration, did not change, or (2) from an empirical relationship between water-column DIC or SO_4^{2-} and K (Baltic sites FB2 and FB13, where salinity increased down-core).

The muddy and silty sites in the Baltic Sea (MB, AB, LB, TW) have the strongest covariation of SO_4^{2-} deficit and DIC, with slopes ranging from −1 to −2.6, with R^2 between 0.86–0.97, suggesting MSR is a key anaerobic pathway of DIC formation in sites with fine-grained sediment (Fig. 6, green points). In sandy North Sea sites, SO_4^{2-} variation is larger than for DIC, suggesting calcification as a possible sink for DIC. In most cases, SO_4^{2-} concentrations are less than bottom water, indicating net consumption by MSR (19, 4, 5, 70, 90). However, there are also sites where some SO_4^{2-} measurements were greater than bottom water (52, 33), suggesting the oxidation of H_2S or FeS_x. This analysis is consistent with aerobic respiration as the major metabolic pathway for net DIC production in ventilated sandy sediments, likely supported by the relatively deep oxygen penetration depths. Interestingly, North Sea mud stations (1 and 26) also have $DIC : SO_4^{2-}$ slopes close to zero (−0.3 and 0.009, respectively). At these sites, while SO_4^{2-} variation is greater than DIC variation, the net change in SO_4^{2-} is still low. This suggests that, even though oxygen penetration depths are low and gross MSR rates are relatively high (Jørgensen, 1989), it is likely that MSR is coupled with internal sulfide oxidation. Potential sources of this sulfate in cases where it appears to be produced (North Sea sites 1, 33, and 52 and Baltic site ST) include sulfide oxidation and FeS_x oxidation, both of which would be increased by intermittent deeper oxygen penetration.

3.4.3 TA sources and sinks: process correlations

We can directly assess the effect of metabolic processes on net TA production for a subset of sites where porewater TA was measured with a sufficient analytical precision. In most of the sandy sites, the down-core variation in TA was less than the analytical precision of the small-volume titrations used. For the sites where porewater TA data are available, TA and DIC are strongly correlated, even in some sandy sites with a much smaller range in both analytes (Fig. 6, orange points). Muddy sites in the Baltic Sea (AB, LB, MB, and the silty TW) have a larger range in both TA and DIC, with slopes (i.e., ratio of TA : DIC) between 0.78 and 1.095. The two sandy Baltic sites (OB and ST) have similar slopes (1.16 and 0.76, respectively), although the range in both variables is much smaller. North Sea Site 1 (muddy) has a slope of 1.12, while the sandy sites have a broad range of 0.13 (Site 2) to 0.65 (Site 5) and 0.8 (Site 4). Modeled DIC fluxes were much larger than TA fluxes for all North Sea sites (Fig. 4; see scale), consistent with measured porewater TA : DIC slopes below 1 : 1 (Fig. 6, orange points).

This is in part due to the likely dominance of aerobic respiration in ventilated North Sea sediments, which in contrast with anaerobic respiration, produces no TA. This dominance of aerobic respiration in permeable North Sea sediment can be attributed to the "redox seal", which describes the situation in percolated sediment with mobile bedforms, where vir-

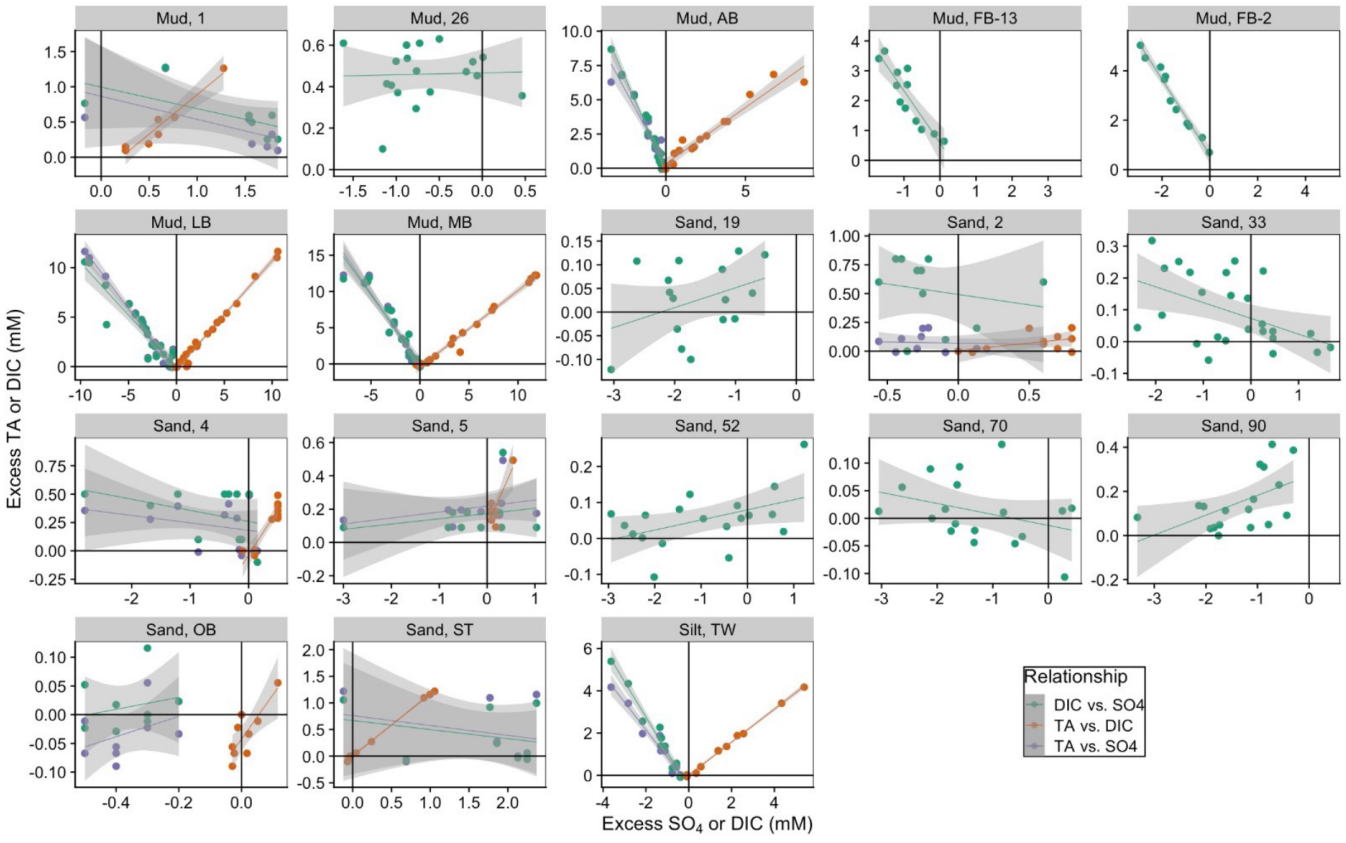

Figure 6. Relationships between excess DIC and excess SO_4^{2-} (green points), excess TA and excess DIC (orange), and excess TA and excess SO_4^{2-} (purple points). Positive values indicate a larger concentration in porewater relative to surface water.

tually the complete percolated sediment layer is oxygenized, whereas transport in the anoxic layer below is restricted to molecular diffusion (Ahmerkamp et al., 2015). Since porewater advection is several orders of magnitude more efficient in the transport of substrates and products than molecular diffusion, fluxes across the sediment surface sustained by aerobic processes substantially exceed those sustained by anaerobic processes. Furthermore, we observe relatively large apparent SO_4^{2-} consumption below the oxic–anoxic interface (Fig. 6, purple points), suggesting significant MSR even in sandy sediments.

Trends between excess TA and apparent SO_4^{2-} consumption are like those for excess DIC (Fig. 6, purple points). Baltic muddy sites have significant ($r^2 > 0.9$) slopes ranging from -1.3 to -2.1. Baltic sandy sites have slopes closer to zero, with small excess TA values, which appear disconnected from apparent SO_4^{2-} reduction. North Sea sandy sites also have slopes closer to zero, and the muddy site (Site 1) has a much shallower slope of -0.3. We infer that iterative carbonate mineral dissolution and precipitation recycling are responsible for our observations of relatively high TA : DIC ratios as well as heavy δ^{13}C-DIC endmembers (Miller–Tans slope). Likewise, we infer microbial SO_4^{2-} reduction is also matched by sulfide oxidation, with little net impact on sediment–water TA fluxes. Together, it appears that strong internal recycling of carbonate minerals and SO_4^{2-} is a major factor causing net TA fluxes to be low across all sites (Table 1).

4 Conclusion

We combined surface water and porewater ^{224}Ra measurements to build a decay balance, which indicates that the irrigative exchange between porewater and surface water is much greater than previously thought. Implicit in this assessment is our finding that the porewater ^{224}Ra endmember was more variable and approximately twice as large as previously assumed; this is of importance for future Ra-based budgets, which are highly sensitive to endmember quantification (Cook et al., 2018; Garcia-Orellana et al., 2021).

In our southern North Sea sites, net sediment–water TA fluxes were very small in comparison with previous estimates in this region (Voyanova et al., 2019; Burt et al., 2014). This is also in contrast to the measured and inferred TA production rates in the Wadden Sea, which are known to be 3–5 orders of magnitude higher on an aerial basis (Santos et al.,

2015), largely associated with substantial net MSR during warm seasons (Al-Raei et al., 2009). TA in ventilated North Sea surface sediments was similar to surface water concentrations, causing net sediment–water fluxes to also be very low ($\sim 10\times$ less than for DIC). Here, TA sources and sinks are closely balanced in North Sea sediments. We ascribe this to the potential influence of (1) DNRA/denitrification being fed internally by recycled, rather than new, NO_3^-; (2) MSR in close balance with sulfide oxidation; and (3) carbonate mineral precipitation in the oxic zone.

In the Baltic Sea sites, excess TA was greater in muddy regions (and close to equilibrium in silty and sandy sites), causing modeled fluxes to be generally low and positive (muddy) or negative (sands) and implying a sink in surficial sediments. At Baltic Sea sites with small positive TA fluxes (muds/silt), net TA production is likely due to net MSR (see sulfate consumption; Fig. 6). In contrast, at sites with net modeled TA uptake (sands), modeling results indicate TA consumption in the uppermost sediment layers, which we attribute to (1) re-oxidation of sulfide and Fe(II); (2) minimal net denitrification, as in North Sea sites; and (3) carbonate mineral precipitation.

Our findings suggest that coastal sediments of the southern North Sea and western Baltic Sea are currently not major sources of TA to the water column. This is because TA production in deeper anaerobic sediments is counter-balanced by re-oxidation and TA consumption in overlying oxic sediment, causing net TA fluxes to be small and variable. The seasonality of these TA fluxes and their impact on water-column carbonate chemistry and ultimately air–water CO_2 exchange were not assessed in this study but should be a topic of future research.

Data availability. All data used in the preparation of this paper, including PROFILE model input and output, are available at the repository figshare (https://doi.org/10.6084/m9.figshare.20134208.v2, Van Dam et al., 2022).

Supplement. The supplement related to this article is available online at: https://doi.org/10.5194/bg-19-3775-2022-supplement.

Author contributions. Conceptualization was by BVD, HT, and MEB. Formal analysis was by BVD, MAZ, and AN. Investigation, inclusive of fieldwork and laboratory work, was by BVD, NL, MAZ, AN, ML, and DP. Project administration, provision of resources, and supervision was by HT, MEB, and DP. Writing of the original draft was by BVD and MAZ. Review and editing was by BVD, NL, MAZ, AN, DP, HT, and MEB.

Competing interests. The contact author has declared that none of the authors has any competing interests.

Disclaimer. Publisher's note: Copernicus Publications remains neutral with regard to jurisdictional claims in published maps and institutional affiliations.

Acknowledgements. The investigations were and are supported by German BMBF projects DAM-MGF (Baltic Sea), CARBOSTORE/COOLSTYLE, and KÜNO SECOS-I/SECOS-II (03F0666 and 03F0738 A–C), as well as German Academic Exchange Service (DAAD) grant no. 57429828 "The Ocean's Alkalinity: Connecting geological and metabolic processes and time-scales", under the BMBF "Make our Planet Great Again – German Research Initiative". This work is contribution no. 001 from the CARBOSTORE/COOLSTYLE consortium (PI Helmuth Thomas). This paper contributes to the science plan of the Surface Ocean-Lower Atmosphere Study (SOLAS), which is supported by the US National Science Foundation via the Scientific Committee on Oceanic Research (SCOR).

Further support was provided by Helmholtz-Zentrum Hereon and the Leibniz Institute for Baltic Sea Research (IOW). We acknowledge the help of D. Bunke, C. Burmeister, F. Cordes, A. Frahm, M. Glockzin, A. Kitte, A. Köhler, G. Lehnert, T. Marquardt, C. Naderipour, S. Plewe, I. Scherff, I. Schmiedinger, M. Norbisrath, B. Rust, L. Schmidt, J. van Beusekom, and T. Zimmermann during field sampling and laboratory analysis. We also thank P. Berg for the helpful discussions about modeling with PROFILE. The authors further wish to thank the captains and crews of R/V *Heincke*, R/V *Elisabeth Mann Borgese*, R/V *Poseidon*, R/V *Alkor*, and R/V *Maria S. Merian* for expert onboard technical support. Finally, we wish to thank Xinping Hu and Perran Cook for their constructive critical reviews, as well as associate editor Jack Middelburg for expertise in handling this submission.

Financial support. This research has been supported by the Deutscher Akademischer Austauschdienst (grant no. 57429828) and the Bundesministerium für Bildung und Forschung (grant nos. 03F0666, 03F0738 A–C, DAM-MGF, and CARBOSTORE).

The article processing charges for this open-access publication were covered by the Helmholtz-Zentrum Hereon.

Review statement. This paper was edited by Jack Middelburg and reviewed by Perran Cook and Xinping Hu.

References

Al-Raei, A. M., Bosselmann, K., Böttcher, M. E., Hespenheide, B., and Tauber, F.: Seasonal dynamics of microbial sulfate reduction in temperate intertidal surface sediments: controls by temperature and organic matter, Ocean Dynam., 59, 351–370, https://doi.org/10.1007/s10236-009-0186-5, 2009.

Ahmerkamp, S., Winter, C., Janssen, F., Kuypers, M. M. M., and Holtappels, M.: The impact of bedform migration on benthic oxygen fluxes, J. Geophys. Res.-Biogeo., 120, 2229–2242, https://doi.org/10.1002/2015JG003106, 2015.

Berelson, W. M., McManus, J., Severmann, S., and Rollins, N.: Benthic fluxes from hypoxia-influenced Gulf of Mexico sediments: Impact on bottom water acidification, Mar. Chem, 209: 94–106, https://doi.org/10.1016/j.marchem.2019.01.004, 2019.

Berg, P., Risgaard-Petersen, N., and Rysgaard, S.: Interpretation of measured concentration profiles in sediment pore water, Limnol. Oceanogr., 43, 1500–1510, https://doi.org/10.4319/lo.1998.43.7.1500, 1998.

Billerbeck, M., Werner, U., Polerecky, L., Walpersdorf, E., DeBeer, D., and Huettel, M.: Surficial and deep pore water circulation governs spatial and temporal scales of nutrient recycling in intertidal sand flat sediment, Mar. Ecol. Prog. Ser., 326, 61–76, https://doi.org/10.3354/meps326061, 2006.

Böttcher, M. E. and Dietzel, M.: Metal-ion partitioning during low-temperature precipitation and dissolution of anhydrous carbonates and sulfates, EMU Notes Mineralog., 10, 139–187, 2010.

Böttcher, M. E., Oelschläger, B., Höpner, T., Brumsack, H.-J., and Rullkötter, J.: Sulfate reduction related to the early diagenetic degradation of organic matter and "black spot" formation in tidal sandflats of the German Wadden Sea: Stable isotope (^{13}C, ^{34}S, ^{18}O) and other geochemical results, Org. Geochem., 29, 1517–1530, 1998.

Böttcher, M. E., Hespenheide, B., Llobet-Brossa, E., Beardsley, C., Larsen, O., Schramm, A., Wieland, A., Böttcher, G., Berninger, U.-G., and Amann, R.: The biogeochemistry, stable isotope geochemistry, and microbial community structure of a temperate intertidal mudflat: An integrated study, Cont. Shelf Res., 20, 1749–1769, 2000.

Borges, A. V., Delille, B., and Frankignoulle, M.: Budgeting sinks and sources of CO_2 in the coastal ocean: Diversity of ecosystem counts, Geophys. Res. Lett., 32, 1–4, https://doi.org/10.1029/2005GL023053, 2005.

Bratek, A., van Beusekom, J. E. E., Neumann, A., Sanders, T., Friedrich, J., Emeis, K.-C., and Dähnke, K.: Spatial variations in sedimentary N-transformation rates in the North Sea (German Bight), Biogeosciences, 17, 2839–2851, https://doi.org/10.5194/bg-17-2839-2020, 2020.

Brenner, H., Braeckman, U., Le Guitton, M., and Meysman, F. J. R.: The impact of sedimentary alkalinity release on the water column CO_2 system in the North Sea, Biogeosciences, 13, 841–863, https://doi.org/10.5194/bg-13-841-2016, 2016.

Burt, W. J., Thomas, H., Pätsch, J., Omar, A. M., Schrum, C., Daewel, U., Brenner, H., and Baar, H. J. W.: Radium isotopes as a tracer of sediment-water column exchange in the North Sea, Global Biochem. Cy., 28, 786–804, https://doi.org/10.1002/2014GB004825, 2014.

Burt, W. J., Thomas, H., Hagens, M., Patsch, J., Clargo, N. M., Salt, L. A., Winde, V., Bottcher, M., Pätsch, J., Clargo, N. M., Salt, L. A., Winde, V., and Böttcher, M. E.: Carbon sources in the North Sea evaluated by means of radium and stable carbon isotope tracers, Limnol. Oceanogr., 61, 666–683, https://doi.org/10.1002/lno.10243, 2016.

Clargo, N. M., Salt, L. A., Thomas, H., and de Baar, H. J. W.: Rapid increase of observed DIC and pCO_2 in the surface waters of the North Sea in the 2001–2011 decade ascribed to climate change superimposed by biological processes, Mar. Chem., 177, 566–581, https://doi.org/10.1016/j.marchem.2015.08.010, 2015.

Cline, J. D.: Spectrophotometric determination of hydrogen sulfide in natural waters, Limnol Oceanogr, 14, 454–458, 1969.

Cook, P. G., Rodellas, V., and Stieglitz, T. C.: Quantifying Surface Water, Porewater, and Groundwater Interactions Using Tracers: Tracer Fluxes, Water Fluxes, and End-member Concentrations, Water Resour. Res., 54, 2452–2465, https://doi.org/10.1002/2017WR021780, 2018.

de Beer, D., Wenzhöfer, F., Ferdelman, T. G., Boehme, S. E., Hüttel, M., van Beusekom, J. E. E., Böttcher, M. E., Musat, N., and Dubilier, N.: Transport and mineralization in North Sea sandy intertidal sediments, Sylt–Rømø Basin, Wadden Sea, Limnol. Oceanogr., 50, 113–127, 2005.

De Borger, E., Braeckman, U., and Soetaert, K.: Rapid organic matter cycling in North Sea sediments, Cont. Shelf Res., 214, 104327, https://doi.org/10.1016/j.csr.2020.104327, 2021.

De Haas, H., Boer, W., and Van Weering, T. C.: Recent sedimentation and organic carbon burial in a shelf sea: The North Sea, Mar. Geol., 144, 131–146. 1997.

Diesing, M., Thorsnes, T., and Bjarnadóttir, L. R.: Organic carbon densities and accumulation rates in surface sediments of the North Sea and Skagerrak, Biogeosciences, 18, 2139–2160, https://doi.org/10.5194/bg-18-2139-2021, 2021. "

Dromgoole, E. L. and Walter, L. M.: Iron and manganese incorporation into calcite: Effects of growth kinetics, temperature and solution chemistry, Chem. Geol., 81, 311–336, 1990.

Garcia-Orellana, J., Rodellas, V., Tamborski, J., Diego-Feliu, M., van Beek, P., Weinstein, Y., Charette, M., Alorda-Kleinglass, A., Michael, H. A., Stieglitz, T., and Scholten, J.: Radium isotopes as submarine groundwater discharge (SGD) tracers: Review and recommendations, Earth-Sci. Rev., 220, 103681, https://doi.org/10.1016/j.earscirev.2021.103681, 2021.

Gustafsson, B.: Interaction between Baltic Sea and North Sea, Dtsch. Hydrogr. Zeitschrift, 49, 165–183, https://doi.org/10.1007/BF02764031, 1997.

Gustafsson, E., Wällstedt, T., Humborg, C., Mörth, C.-M., and Gustafsson, B. G.: External total alkalinity loads versus internal generation: The influence of nonriverine alkalinity sources in the Baltic Sea, Global Biogeochem. Cy., 28, 1358–1370, https://doi.org/10.1002/2014GB004888, 2014.

Gogina, M., Lipka, M., Woelfel, J., Liu, B., Morys, C., Böttcher, M. E., and Zettler, M. L.: In Search of a Field-Based Relationship Between Benthic Macrofauna and Biogeochemistry in a Modern Brackish Coastal Sea, Front. Mar. Sci., 5, 1–18, https://doi.org/10.3389/fmars.2018.00489, 2018.

Graßhoff, K. and Almgren, T.: Methods of seawater analysis, 2., rev., and extended edn., Verl. Chemie, Weinheim, 419 pp, 1983.

Hagens, M., Slomp, C. P., Meysman, F. J. R., Seitaj, D., Harlay, J., Borges, A. V., and Middelburg, J. J.: Biogeochemical processes and buffering capacity concurrently affect acidification in a seasonally hypoxic coastal marine basin, Biogeosciences, 12, 1561–1583, https://doi.org/10.5194/bg-12-1561-2015, 2015.

Jørgensen, B. B.: Sulfate reduction in marine sediments from the baltic sea-north sea transition, Ophelia, 31, 1–15, https://doi.org/10.1080/00785326.1989.10430847, 1989.

Ku, T. C. W., Walter, L. M., Coleman, M. L., Blake, R. E., and Martini, A. M.: Coupling between sulfur recycling and syndepositional carbonate dissolution: Evidence from oxygen and sulfur isotope composition of pore water sulfate, South Florida Platform, U. S. A., Geochim. Cosmochim. Ac., 63, 2529–2546, https://doi.org/10.1016/S0016-7037(99)00115-5, 1999.

Kuliński, K., Rehder, G., Asmala, E., Bartosova, A., Carstensen, J., Gustafsson, B., Hall, P. O. J., Humborg, C., Jilbert, T., Jürgens, K., Meier, H. E. M., Müller-Karulis, B., Naumann, M., Olesen, J. E., Savchuk, O., Schramm, A., Slomp, C. P., Sofiev, M., Sobek, A., Szymczycha, B., and Undeman, E.: Biogeochemical functioning of the Baltic Sea, Earth Syst. Dynam., 13, 633–685, https://doi.org/10.5194/esd-13-633-2022, 2022.

Lacroix, F., Ilyina, T., Laruelle, G. G., and Regnier, P.: Reconstructing the Preindustrial Coastal Carbon Cycle Through a Global Ocean Circulation Model: Was the Global Continental Shelf Already Both Autotrophic and a CO_2 Sink?, Global Biogeochem. Cy., 35, 1–23, https://doi.org/10.1029/2020GB006603, 2021.

Laruelle, G. G., Dürr, H. H., Slomp, C. P., and Borges, A. V.: Evaluation of sinks and sources of CO_2 in the global coastal ocean using a spatially-explicit typology of estuaries and continental shelves, Geophys. Res. Lett., 37, https://doi.org/10.1029/2010GL043691, 2010.

Laruelle, G. G., Cai, W. J., Hu, X., Gruber, N., Mackenzie, F. T., and Regnier, P.: Continental shelves as a variable but increasing global sink for atmospheric carbon dioxide, Nat. Commun., 9, 1–11, https://doi.org/10.1038/s41467-017-02738-z, 2018.

Lenstra, W. K., Hermans, M., Séguret, M. J. M., Witbaard, R., Severmann, S., and Slomp, C. P.: Hypoxia and eutrophication as key controls on benthic release and water column dynamics of iron and manganese in the Baltic Sea, Limnol. Oceanogr., 66, 807–826, https://doi.org/10.1002/lno.11644, 2019.

Lipka, M.: Current biogeochemical processes and element fluxes in surface sediments of temperate marginal seas (Baltic Sea and Black Sea), PhD thesis, https://nbn-resolving.org/urn:nbn:de:gbv:9-opus-23761 (last access: 13 January 2022), 2017.

Lipka, M., Woelfel, J., Gogina, M., Kallmeyer, J., Liu, B., Morys, C., Forster, S., and Böttcher, M. E.: Solute reservoirs reflect variability of early diagenetic processes in temperate brackish surface sediments, Front. Mar. Sci., 9, 1–20, https://doi.org/10.3389/fmars.2018.00413, 2018.

Maar, M., Møller, E. F., Larsen, J., Madsen, K. S., Wan, Z., She, J., Jonasson, L., and Neumann, T.: Ecosystem modelling across a salinity gradient from the North Sea to the Baltic Sea, Ecol. Modell., 222, 1696–1711, https://doi.org/10.1016/j.ecolmodel.2011.03.006, 2011.

Marchant, H. K., Holtappels, M., Lavik, G., Ahmerkamp, S., Winter, C., and Kuypers, M. M. M.: Coupled nitrification – denitrification leads to extensive N loss in subtidal permeable sediments, Limnol. Oceanogr., 61, 1033–1048, https://doi.org/10.1002/lno.10271, 2016.

Meister, P., Liu, B., Khalili, A., Böttcher, M. E., and Jørgensen, B. B.: Factors controlling the carbon isotope composition of dissolved inorganic carbon and methane in marine porewater: An evaluation by reaction-transport modelling, J. Mar. Syst., 200, 103227, https://doi.org/10.1016/j.jmarsys.2019.103227, 2019.

Meyer, M., Pätsch, J., Geyer, B., and Thomas, H.: Revisiting the Estimate of the North Sea Air–Sea Flux of CO_2 in 2001/2002: The Dominant Role of Different Wind Data Products, J. Geophys. Res.-Biogeo., 123, 1511–1525, https://doi.org/10.1029/2017JG004281, 2018.

Moore, W. S. and Arnold, R.: Measurement of ^{223}Ra and ^{224}Ra in coastal waters using a delayed coincidence counter, J. Geophys. Res.-Oceans, 101, 1321–1329, https://doi.org/10.1029/95JC03139, 1996.

Moore, W. S., Beck, M., Riedel, T., Rutgers van der Loeff, M., Dellwig, O., Shaw, T. J., Schnetger, B., and Brumsack, H. J.: Radium-based pore water fluxes of silica, alkalinity, manganese, DOC, and uranium: A decade of studies in the German Wadden Sea, Geochim. Cosmochim. Ac., 75, 6535–6555, https://doi.org/10.1016/j.gca.2011.08.037, 2011.

Morse, J. W. and Mackenzie, F. T.: Geochemistry of sedimentary carbonates, Elsevier, 1990.

Neumann, A., van Beusekom, J. E. E., Holtappels, M., and Emeis, K.: Nitrate consumption in sediments of the German Bight (North Sea), J. Sea Res., 127, 26–35, https://doi.org/10.1016/j.seares.2017.06.012, 2017.

Neumann, A., van Beusekom, J. E. E., Eisele, A., Emeis, K. C., Friedrich, J., Kröncke, I., Logemann, E. L., Meyer, J., Naderipour, C., Schückel, U., Wrede, A., and Zettler, M. L.: Macrofauna as a major driver of bentho-pelagic exchange in the southern North Sea, Limnol. Oceanogr., 66, 2203–2217, https://doi.org/10.1002/lno.11748, 2021.

Pätsch, J., Kühn, W., and Six, K. D.: Interannual sedimentary effluxes of alkalinity in the southern North Sea: model results compared with summer observations, Biogeosciences, 15, 3293–3309, https://doi.org/10.5194/bg-15-3293-2018, 2018.

Pollmann, T., Böttcher, M. E., and Giani, L.: Young soils of a temperate barrier island under impact of formation and resetting by tides and wind, Catena, 202, 105275, https://doi.org/10.1016/j.catena.2021.105275, 2021.

Rassmann, J., Eitel, E. M., Lansard, B., Cathalot, C., Brandily, C., Taillefert, M., and Rabouille, C.: Benthic alkalinity and dissolved inorganic carbon fluxes in the Rhône River prodelta generated by decoupled aerobic and anaerobic processes, Biogeosciences, 17, 13–33, https://doi.org/10.5194/bg-17-13-2020, 2020.

Reithmaier, G. M. S., Johnston, S. G., Junginger, T., Goddard, M. M., Sanders, C. J., Hutley, L. B., Ho, D. T., and Maher, D. T.: Alkalinity Production Coupled to Pyrite Formation Represents an Unaccounted Blue Carbon Sink, Global Biogeochem. Cy., 35, 1–20, https://doi.org/10.1029/2020GB006785, 2021.

Rutherford, K., Fennel, K., Atamanchuk, D., Wallace, D., and Thomas, H.: A modelling study of temporal and spatial pCO_2 variability on the biologically active and temperature-dominated Scotian Shelf, Biogeosciences, 18, 6271–6286, https://doi.org/10.5194/bg-18-6271-2021, 2021.

Santos, I. R., Beck, M., Brumsack, H. J., Maher, D. T., Dittmar, T., Waska, H., and Schnetger, B.: Porewater exchange as a driver of carbon dynamics across a terrestrial-marine transect: Insights from coupled ^{222}Rn and pCO_2 observations in the German Wadden Sea, Mar. Chem., 171, 10–20, https://doi.org/10.1016/j.marchem.2015.02.005, 2015.

Schwichtenberg, F., Pätsch, J., Böttcher, M. E., Thomas, H., Winde, V., and Emeis, K.-C.: The impact of intertidal areas on the carbonate system of the southern North Sea, Biogeosciences, 17, 4223–4245, https://doi.org/10.5194/bg-17-4223-2020, 2020.

Serna, A., Lahajnar, N., Pätsch, J., Hebbeln, D., and Emeis, K. C, Organic matter degradation in the German Bight/SE North Sea: Implications from stable nitrogen isotopes and amino acids, Mar. Chem., 166, 103–113, https://doi.org/10.1016/j.marchem.2014.09.014, 2014.

Thomas, H., Bozec, Y., Elkalay, K., and De Baar, H. J. W.: Enhanced Open Ocean Storage of CO_2

from Shelf Sea Pumping, Science, 304, 1005–1008, https://doi.org/10.1126/science.1095491, 2004.

Thomas, H., Prowe, A. E. F., van Heuven, S., Bozec, Y., de Baar, H. J. W., Schiettecatte, L. S., Suykens, K., Koné, M., Borges, A. V., Lima, I. D., and Doney, S. C.: Rapid decline of the CO_2 buffering capacity in the North Sea and implications for the North Atlantic Ocean, Global Biogeochem. Cy., 21, 1–13, https://doi.org/10.1029/2006GB002825, 2007.

Thomas, H., Schiettecatte, L.-S., Suykens, K., Koné, Y. J. M., Shadwick, E. H., Prowe, A. E. F., Bozec, Y., de Baar, H. J. W., and Borges, A. V.: Enhanced ocean carbon storage from anaerobic alkalinity generation in coastal sediments, Biogeosciences, 6, 267–274, https://doi.org/10.5194/bg-6-267-2009, 2009.

Van Dam, B., Lehmann, N., Zeller, M. A., Neumann, A., Pröfrock, D., Lipka, M., Thomas, H., and Böttcher, M. E.: Baltic – North Sea, figshare [data set], https://doi.org/10.6084/m9.figshare.20134208.v2, 2022.

van den Berg, C. M. G. and Rogers, H.: Determination of alkalinities of estuarine waters by a two-point potentiometric titration, Mar. Chem., 20, 219–226, 1987.

Voß, M. and Struck, U.: Stable nitrogen and carbon isotopes as indicator of eutrophication of the Oder river (Baltic sea), Mar. Chem., 59, 35–49, https://doi.org/10.1016/S0304-4203(97)00073-X, 1997.

Voynova, Y. G., Petersen, W., Gehrung, M., Aßmann, S., and King, A. L.: Intertidal regions changing coastal alkalinity: The Wadden Sea-North Sea tidally coupled bioreactor, Limnol. Oceanogr., 64, 1135–1149, https://doi.org/10.1002/lno.11103, 2019.

Walter, L. M., Ku, T. C. W., Muehlenbachs, K., Patterson, W. P., and Bonnell, L.: Controls on the $\delta^{13}C$ of dissolved inorganic carbon in marine pore waters: An integrated case study of isotope exchange during syndepositional recrystallization of biogenic carbonate sediments (South Florida Platform, USA), Deep-Sea Res. Pt. II, 54, 1163–1200, https://doi.org/10.1016/j.dsr2.2007.04.014, 2007.

Winde, V., Böttcher, M. E., Escher, P., Böning, P., Beck, M., Liebezeit, G., and Schneider, B.: Tidal and spatial variations of $DI^{13}C$ and aquatic chemistry in a temperate tidal basin during winter time, J. Mar. Sys, 129, 394–402, 2014a.

Winde, V., Escher, P., Schneider, B., Böning, P., Al-Raei, A. M., Liebezeit, G., and Böttcher, M. E.: Carbon isotopes in DIC trace submarine groundwater discharge and advective pore water efflux in tidal areas of the southern North Sea, Proc. 23rd SWIM conference, Husum, 16–20 June 2014, 42–45, ISBN 978-3-00-046061-6, 2014b.

Winde, V., Böttcher, M. E., Voss, M., and Mahler, A.: Bladder wrack (Fucus vesiculosus) as a multi-isotope bio-monitor in an urbanized fjord of the western Baltic Sea, Isot. Environ. Health Stud., 53, 563–579, https://doi.org/10.1080/10256016.2017.1316980, 2017.

Wu, Z., Liu, B., Escher, P., Kowalski, N., and Böttcher, M. E.: Carbon diagenesis in different sedimentary environments of the subtropical Beibu Gulf, South China Sea, J. Marine Syst., 186, 68–84, 2018.

Zeebe, R. E. and Wolf-Gladrow, D.: CO_2 in seawater: equilibrium, kinetics, isotopes, No. 65, Gulf Professional Publishing, 2001.

Zimmermann, T., Von Der Au, M., Reese, A., Klein, O., Hildebrandt, L., and Pröfrock, D.: Substituting HF by HBF4-an optimized digestion method for multi-elemental sediment analysis: Via ICP-MS/MS, Anal. Methods-UK, 12, 3778–3787, https://doi.org/10.1039/d0ay01049a, 2020.